Available online at www.sciencedirect.com
SCIENCE DIRECT®
Journal of Power Sources 144 (2005) 302–309
JOURNAL OF POWER SOURCES
www.elsevier.com/locate/jpowsour

Effects of pore structure and electrolyte on the capacitive characteristics of steam- and KOH-activated carbons for supercapacitors

Feng-Chin Wu[a,*], Ru-Ling Tseng[b], Chi-Chang Hu[c], Chen-Ching Wang[c]

[a] *Department of Chemical Engineering, National United University, No.1, Lien Da, Kung-Ching Li, Miao-Li 360, Taiwan*
[b] *Department of Safety, Health and Environmental Engineering, National United University, Miao-Li 360, Taiwan*
[c] *Department of Chemical Engineering, National Chung Cheng University, Chia-Yi 621, Taiwan*

Received 25 October 2004; received in revised form 19 December 2004; accepted 19 December 2004
Available online 6 February 2005

Abstract

Four kinds of activated carbons (denoted as ACs) with specific surface area of ca. 1050 $m^2\ g^{-1}$ were fabricated from fir wood and pistachio shell by means of steam activation or chemical activation with KOH. Pore structures of ACs were characterized by a t-plot method based on N_2 adsorption isotherms. The amount of mesopores within KOH-activated carbons ranged from 9.2 to 15.3% while 33.3–49.5% of mesopores were obtained for the steam-activated carbons. The pore structure, surface functional groups, and raw materials of ACs, as well as pH and the supporting electrolyte were also found to be significant factors determining the capacitive characteristics of ACs. The excellent capacitive characteristics in both acidic and neutral media and the weak dependence of the specific capacitance on the scan rate of cyclic voltammetry (CV) for the ACs derived from the pistachio shell with steam activation (denoted as P-H_2O-AC) revealed their promising potential in the application of supercapacitors. The ACs derived from fir wood with KOH activation (denoted as F-KOH-AC), on the other hand, showed the best capacitive performance in H_2SO_4 due to excellent reversibility and high specific capacitance (180 F g^{-1} measured at 10 mV s^{-1}), which is obviously larger than 100 F g^{-1} (a typical value of activated carbons with specific surface areas equal to/above 1000 $m^2\ g^{-1}$).

Keywords: Activated carbon; Steam activation; KOH activation; Pore structure; Surpercapacitor

1. Introduction

The physicochemical properties, including specific surface area, pore volume, and porosity, of activated carbons (ACs) were found to be a strong function of the activation process and method as well as the nature of raw materials [1,2]. In addition, an understanding of the influences of activation variables in both physical and chemical activation processes on the physicochemical properties of ACs is very important in manufacturing carbons with a desired structure [1]. This is especially important in the development of micro- and mesopores because they are strongly related to the adsorption capability and ability of carbons for various types of chemicals from gas or liquids. Accordingly, recent research has focused on the development of ACs with desired pore structures and on new applications [3].

Activated carbons are important industrial materials for various applications [4–8]. Recently, investigations of the relationship between the porous structures and electrochemical behavior became important because they have been widely recognized as an electrode material for surpercapacitors [4,9–11]. Since the cost of AC-based supercapacitors (i.e., electric double layer capacitors (EDLCs)) is low [10], this type of energy storage devices is commercially attractive for many applications, such as mobile telecommunictions, starting and back-up power for engines, etc. [12]. On the other hand, for high-power, the proportion of mesopores (i.e., 50 nm > pore diameter > 2 nm) within ACs is considered to be one of the key factors determining the capacitive

* Corresponding author. Tel.: +886 37 381575; fax: +886 37 332397.
E-mail address: wfc@nuu.edu.tw (F.-C. Wu).

0378-7753/$ – see front matter © 2005 Elsevier B.V. All rights reserved.
doi:10.1016/j.jpowsour.2004.12.020

performance of EDLCs since a complete array of the electric double layers can be established and solvated ions can move freely within such pores although a high proportion of mesopores will result in a loss of specific surface area [11,13].

A large portion of electric energy stored in supercapacitors will be consumed during discharge if the equivalent series resistance (ESR) is significant, usually resulting from the poor conductivity of ACs as well as the poor diffusion of solvated ions within micropores [9,12,14]. These characteristics depend mainly on the nature, the BET surface, and the porous structure of carbons [9,12,13–15]. Accordingly, the pore size distribution is believed to be one of the key factors that dictate the selection of ACs for EDLCs [9,10,12]. In fact, ACs manufactured under different conditions were found to have different pore structures and surface conditions, usually resulting in an incomplete utilization of the surface area (i.e., electrochemically inaccessible/partially accessible) [9,12–14]. In addition, to the accessible surface areas, the capacitance per unit area (in $\mu F\,cm^{-2}$) is not the same due to the presence of various functional groups [13,16]. Hence, several studies were carried out to modify the surface properties of ACs in order to optimize their capacitive performance (i.e., high-power, low ESR and high specific capacitance) [4,6–11,14–16]. A typical value of specific capacitance of around $120\,F\,g^{-1}$ for carbons with careful selection [11] was proposed to be a promising and practical material for this application.

In general, AC materials with unique pore size distributions usually result from the differences in precursors and activations [13,17]. In addition, a relative high proportion of mesopores (i.e., high proportion of the electrochemically accessible surface area) within these materials, the typical characteristics of wood-derived ACs is required for supercapacitor applications [5]. In our previous work [5,18,19], a series of studies were conducted to manufacture ACs with a unique pore size distribution (from wood wastes and shells), which were evaluated for the possibility for pollution control. The aim of this paper is to prepare various ACs with different pore size distributions and to evaluate their applicability to supercapacitors. In addition, the physicochemical properties, including the BET surface area, pore size distribution, total pore volume, yield, and surface functional groups, of steam- and KOH-activated carbons were systematically characterized and correlated to their capacitive properties.

2. Experimental details

2.1. Preparation of steam-activated carbons

The fir wood employed in this work came from fir trees, which was used as an instrument jacket. The firs (a genus of evergreen conifers in the family Pinaceae) should belong to *Abies bifolia* in North America. The received raw materials were dried at 110 °C for 24 h and then, placed in a sealed ceramic oven and heated at a rate of $5\,^{\circ}C\,min^{-1}$ to 550 °C. In the meantime, steam generated from deionized water (Millipore, Milli-Q) in a heated tube was poured into the oven at a rate of $3\,cm^3\,min^{-1}$ for 3 and 2 h, respectively, for fir wood and pistachio shells. After this step, they were carbonized at 550 °C in an oxygen-deficient environment. In the subsequent activation process, the oven was further heated at the same rate to 900 and 890 °C, respectively, under the same flow-rate of steam. The times for activation at 900 and 890 °C were 5 and 3 h, respectively. The resultant carbons were ground in a mill followed by washing with pure water and drying. Finally, these steam-activated carbons were sieved in the size range 0.12–0.2 mm, and are denoted as W-H_2O-AC and P-H_2O-AC for those prepared from fir wood and pistachio shells, respectively.

2.2. Preparation of KOH-activated carbons

Chars of fir wood and pistachio shells prepared by the carbonization process in Section 2.1 were removed, crushed, and sieved to a uniform size range from 0.833 to 1.65 mm. A solution of chars, KOH, and H_2O (in the 1:1:1 weight ratio) was well agitated in a stainless steel beaker. After drying at 130 °C for 24 h, the chars, placed in a sealed ceramic oven were heated at a rate of $10\,^{\circ}C\,min^{-1}$ to 780 °C and maintained at this temperature for 1 h. During this activation process, N_2 gas was flowed into the oven by a rate of $4\,dm^3\,min^{-1}$. The activated products were then cooled to room temperature and washed with deionized water. Subsequently, the samples were transferred into 0.1 M HCl ($250\,cm^3$), stirred for 1 h, and washed with hot deionized water until pH of the washed solution was about 6–7 [20]. Finally, they were dried in a vacuum oven at room temperature for 24 h. These KOH-activated carbons prepared from fir wood and pistachio shells are denoted as W-KOH-AC and P-KOH-AC, respectively.

2.3. Measurements of physical properties

The yield of activated carbons is defined as the weight ratio of final carbons to the initial dried raw materials. The BET surface area of carbons (S_p) was obtained from N_2 adsorption isotherms at 77 K (Porous Materials, BET-202A). The total pore volume (V_{pore}) and pore size distribution were obtained by the BJH theory [21] in the same equipment. The micropore volume (V_{micro}) and external surface area (S_{ext}) were obtained using the *t*-plot method [22–24]. The surface area corresponding to micropores (S_{micro}) was obtained by difference [25].

2.4. Electrode preparation

Activated carbon powders were well mixed with the 2 wt.% PVdF binders for 30 min and *N*-methyl-2-pyrrolidone (NMP) was dropped into the above mixture and ground to form the coating slurry. This slurry was smeared onto the pretreated graphite substrates and dried in a vacuum oven at 50 °C overnight. In order to avoid any unexpected

influences, the total amount of AC pastes on each electrode was kept approximately constant (ca. 2 mg cm^{-2}). The 10 mm × 10 mm × 3 mm graphite substrates before coating with ACs were first abraded with ultrafine SiC paper, degreased with acetone and water, then etched in a 0.1 M HCl solution at room temperature (ca. 26 °C) for 10 min, and finally degreased with water in an ultrasonic bath. The exposed geometric area of these pretreated graphite supports is equal to 1 cm^2 while the other surface areas were insulated with PTFE (polytetrafluorene ethylene) coatings.

2.5. Capacitance measurements

Cyclic voltammetry (CV) was performed by an electrochemical analyzer system, CHI 633A (CH Instruments) between −0.1 and 0.9 V. All experiments were carried out in a three-compartment cell. An Ag/AgCl electrode (Argenthal, 3 M KCl, 0.207 V versus SHE at 25 °C) was used as the reference and a platinum wire with an exposed area equal to 4 cm^2 was employed as the counter electrode. A Luggin capillary was used to minimize errors due to *iR* drop in the electrolytes. The electrolytes used for the capacitive characterization were degassed with purified nitrogen gas before measurements for 25 min and this nitrogen was passed over the solutions during the measurements. The solution temperature was maintained at 25 °C by means of a water thermostat (Haake DC3 and K20).

3. Results and discussion

3.1. Physical properties of steam- and KOH-activated carbons

Identifying the microstructure is an essential procedure for designing and developing activated carbons. In addition, the establishment of electric double layers should be strongly dependent on the intrinsic pore size distribution of ACs [9,12,13,17] although micropores usually account for over 95% of the total surface area for common AC materials [26]. Accordingly, the pore size distribution and the proportion of micro-/mesopores within ACs are very important to the application of supercapacitors. Based on the definition from IUPAC, pores distributed within ACs are classified into three groups: micropores (pore size < 2 nm), mesopores (2–50 nm), and macropores (>50 nm), which can be suitably evaluated by the adsorption isotherms of inert gases (e.g., N_2 and He) [27].

Typical adsorption/desorption isotherms of N_2 at 77 K onto W-H_2O-AC, P-H_2O-AC, W-KOH-AC, and P-KOH-AC are shown in Fig. 1 as curves 1–4, respectively. For curves 1 and 2 (i.e., the steam-activated carbons), adsorption and desorption lines overlap completely in the low relative-pressure region while a hysterestic loop is clearly found in the high relative-pressure region ($P/P_0 > 0.5$). This loop has been mainly attributed, among other factors such as the slit-shaped

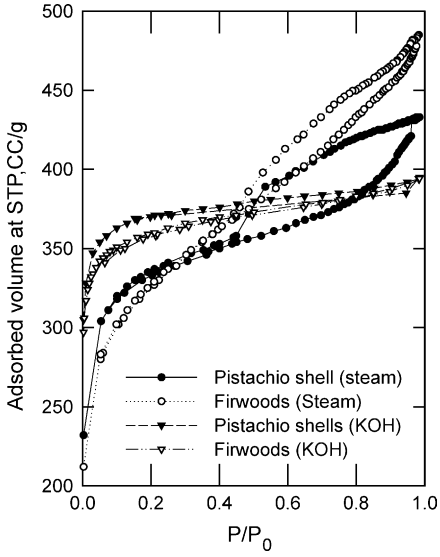

Fig. 1. Adsorption/desorption isotherms of N_2 at 77 K on (1, ◯) W-H_2O-AC; (2, ●) P-H_2O-AC; (3, ▽) W-KOH-AC and (4, ▼) P-KOH-AC.

pores, to the presence of ink-bottle type of pores [28]. According to the Kelvin equation [29], pores of the ink-bottle type are large, resulting in the presence of a hysteresis loop in the high relative-pressure region. A feature common to many hysteresis loops is that the steep region of the desorption branch can be associated with the lower closure point and occurs (for a given adsorptive at a given temperature) at a relative pressure which is almost independent of the nature of the porous adsorbent but depends mainly on the nature of the adsorptive (e.g., for nitrogen at its boiling point at $P/P_0 \approx 0.42$ and for benzene at 25 °C at $P/P_0 \approx 0.28$) [29]. On the other hand, the isotherms for KOH-activated carbons (see curves 3 and 4) show the general features of Type-I (Langmuir type) adsorption [29]. In general, microporous solids with relatively small external surfaces generally show the Type-I adsorption isotherms [29]. In addition, the initial (steep) part of a Type-I isotherm represents the micropore filling (rather than the surface coverage) and the low slope of plateau is due to the multilayer adsorption on the external surface area [29]. Based on the above results and discussion, the pore size distribution and structure are undoubtedly determined by the activation methods although they also depend on the source of raw materials.

The pore size distributions of W-H_2O-AC, P-H_2O-AC, W-KOH-AC, and P-KOH-AC are shown in Fig. 2 as curves 1–4, respectively, where D_P indicates the pore diameter. There is a peak at $D_P < 2$ nm and another peak is found as D_P between 3.5 and 4.5 nm for the steam-activated carbons (see curves 1 and 2). Accordingly, the steam activation develops the pores of two distributions corresponding to the micropores and mesopores, respectively. On the contrary, the KOH activation method produces the pore size distribution located in the micropore range.

The pore properties of W-H_2O-AC, P-H_2O-AC, W-KOH-AC, and P-KOH-AC, including S_P, S_{micoro}/S_P, V_{pore},

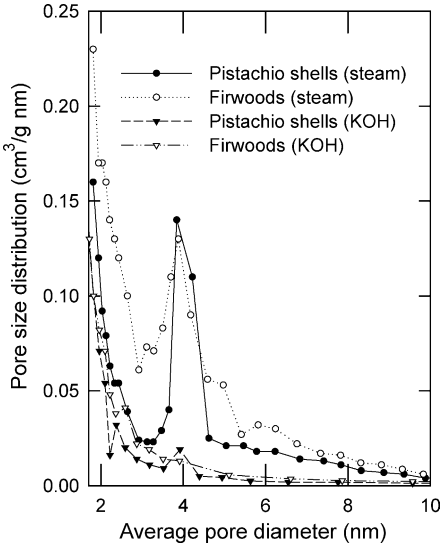

Fig. 2. Pore size distribution of (1, ◯) W-H_2O-AC; (2, ●) P-H_2O-AC; (3, ▽) W-KOH-AC and (4, ▼) P-KOH-AC.

V_{micro}/V_{pore}, D_P, and yield, are listed in Table 1. Note that in order to avoid the influence of specific surface area (S_P) on the specific capacitance (studied in Section 3.3), the specific surface areas of all carbons are carefully controlled in the range from 1009 to1096 $m^2\,g^{-1}$. In addition, the S_P of ACs prepared in this work is comparable to those of commercial ones; for example, 300–600 (ICI Hydrodarco 3000), 1044 (Calgon Filtrasorb 400), 1000 (Westvaco Nuchar WL), and 1050 $m^2\,g^{-1}$ (Witco 517) although the specific surface area of some ACs prepared by chemical activation was found to reach 2500 $m^2\,g^{-1}$ or above [30,31]. Moreover, carbons prepared from apricot stones, grape seeds, and cherry stones have S_P of 1175, 487, and 836 $m^2\,g^{-1}$, respectively [32].

The ratios between the surface area of micropores and the total specific surface area, S_{micoro}/S_P, for W-KOH-AC and P-KOH-AC are 0.926 and 0.941, respectively, which are larger than those of steam-activated carbons (i.e., 0.700 and 0.859 for W-H_2O-AC and P-H_2O-AC, respectively). This result shows that the KOH activation method is a powerful procedure to produce carbons enriched with micropores while the steam activation method prefers to develop the external surface area. The mircropore volume ratios, V_{micro}/V_{pore}, of KOH- and steam-activated carbons are from 0.843 to 0.908 and from 0.505 to 0.667, respectively, supporting the result that the KOH activation method prefers to produce ACs enriched with micropores. Note that the mean diameter of W-KOH-AC and P-KOH-AC is equal to 2.28 and 2.22 nm, respectively, which is respectively smaller than that of their corresponding counterparts activated by steam (2.94 and 2.64 nm for W-H_2O-AC and P-H_2O-AC, respectively). The above comparisons indicate that the steam activation method is able to develop the pores with a larger mean D_P. In fact, the D_P data of steam-activated carbons are larger than that of some commercially available ACs (0.912–2.30 nm), such as 0.912 (Spectracorp M-10), 1.473 (Spectracorp M-20), 2.23 (Calgon F400), 2.0 (Barney Cheney SK1301), 1.90 (Westvaco Nuchar MV-L) and 2.30 nm (Westvco WV-DC). In addition, the average pore diameter of ACs prepared from coconut shells, palm seeds, bagasse and plum kernel were 2.1, 2.43, 1.46, and 2.39 nm, respectively [5,19,33]. Due to the fact that mean D_P of steam-activated carbons prepared in this work is relatively large (from 2.64 to 2.94 nm), these carbons were expected to show ideal capacitive performance in both neutral and acidic electrolytes. The yield of W-H_2O-AC and W-KOH-AC is equal to 10.35 and 14.93%, respectively, meanwhile that of P-H_2O-AC and P-KOH-AC is equal to 13.59 and 22.72%, respectively. These results show that the yields of ACs derived from fir wood and pistachio shells by the chemical method are 1.44 and 1.67 times of those through means of the physical method. The yields of chemically activated carbons are usually higher than the physically activated counterparts because the chemical agents used in the former cases are dehydrogenation substances that inhibit the formation of tar and reduce the production of other volatile products [1,34,35]. In addition, the chemical activation process usually shows an important advantage that the activation process normally takes place at lower temperatures and shorter times in comparing with those used in the physical activation [1].

3.2. Identifying the surface functional groups of steam- and KOH-activated carbons via TPD

The main surface functional groups present in the char were carbonyl groups (e.g., Ketone and quinone) and aromatic rings [36–38], such as found on the chars derived from peach stone [36], roockose [37], and oil-palm stones [38]. For ACs prepared at high temperatures (e.g., 900 °C) and long activation time (e.g., 60 min), only aromatic rings remained [38]. These surface organic functional groups were generally neutral (or slightly acidic), which should not have a significant influence on the adsorptive capacity of ACs [38]. However, the distribution of surface functional groups is usually a function of the preparation variables for the chemically activated carbons, significantly influencing their specific capacitance. Based on this reason, the surface functional groups

Table 1
Physical properties and activated condition of activated carbons prepared from fir wood and pistachio shell

Activated carbons	Source	Activation agent	T_A (°C)	t_A (h)	S_P ($m^2\,g^{-1}$)	S_{micro}/S_P	V_{pore} ($cm^3\,g^{-1}$)	V_{micro}/V_{pore}	D_P (nm)	Yield
W-H_2O-AC	Fir wood	Steam	900	5	1016	0.700	0.747	0.505	2.94	10.35
P-H_2O-AC	Pistachios shell	Steam	890	3	1009	0.859	0.667	0.667	2.64	13.59
W-KOH-AC	Fir wood	KOH	780	1	1064	0.926	0.607	0.843	2.28	14.93
P-KOH-AC	Pistachios shell	KOH	780	1	1096	0.941	0.608	0.908	2.22	22.72

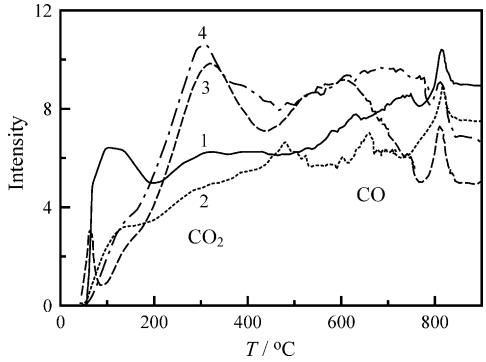

Fig. 3. Evolution profiles of CO_2 and CO by temperature programmed desorption for (1) W-H_2O-AC, (2) P-H_2O-AC, (3) W-KOH-AC, and (4) P-KOH-AC.

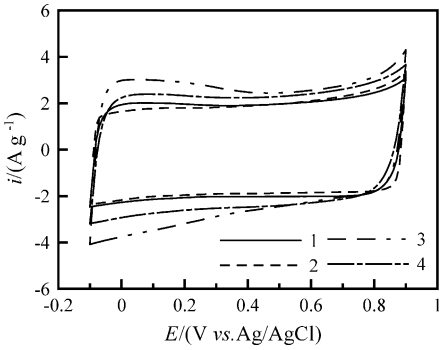

Fig. 4. Cyclic voltammograms of (1) W-H_2O-AC, (2) P-H_2O-AC, (3) W-KOH-AC, and (4) P-KOH-AC measured at 20 mV s^{-1} in 1.0 M $NaNO_3$.

of all ACs were roughly analyzed by means of temperature-programming desorption (TPD) [39] in this work. Typical evolution profiles of CO_2 and CO determined by the TPD method for W-H_2O-AC, P-H_2O-AC, W-KOH-AC, and P-KOH-AC are shown as curves 1–4, respectively in Fig. 3.

It is well known that CO_2 mainly desorbs at relatively low temperatures (i.e., <550 °C), which has been attributed to the presence of anhydrides, lactones, and carboxyl groups [13,39,40]. On the other hand, desorption of CO species, attributable to quinone, hydroxyl, and carbonyl groups, occurs predominately at relatively higher temperatures (ca. >500 °C) [13,39,40]. Thus, the distribution of oxygen functional groups can be estimated from the TPD results. An examination of all curves in Fig. 3 indicates several features. First, the relative intensities of CO_2 and CO desorption (especially for CO_2 desorption) were increased with the chemical activation of KOH (see curves 3 and 4). Second, the total density of functional groups on the P-KOH-AC should be the highest among these four types of carbons. Third, the intensities of CO desorption are higher than that of CO_2 desorption for the steam-activated carbons, suggesting that the steam-activated carbons should be enriched with the quinone, hydroxyl, or carbonyl groups. The KOH-activated carbons, however, were enriched in all kinds of oxygen functional groups. Based on the above descriptions, evolution of CO_2 and CO is visible for all ACs prepared in this work while the distribution of surface oxygen functional groups is functions of the activation method and the raw material.

3.3. Capacitive performance of steam- and KOH-activated carbons

Typical cyclic voltammetric behavior of W-H_2O-AC, P-H_2O-AC, W-KOH-AC, and P-KOH-AC measured at 20 mV s^{-1} in 1.0 M $NaNO_3$ is shown in Fig. 4 as curves 1–4, respectively. Note that the background currents on all curves are of the same order, indicating that the specific surface area of ACs is the predominant factor determining the specific capacitance of AC-pasted electrodes. Accordingly, double-layer charge/discharge dominates the energy storage process on these electrodes (i.e., suitable for the application of EDLCs). Also note that all CV curves are rectangular-like without obvious redox currents on both positive and negative sweeps in the whole potential range of investigation. These capacitive-like and symmetric *i–E* responses indicate that $NaNO_3$ is a suitable electrolyte in the EDLC application for both steam-activated and KOH-activated carbons and that the capacitive characteristics of all carbons are excellent although the pore structures and the distributions of surface oxygen functional groups on these ACs are different. Based on the fact that the voltammetric charges on the positive and negative sweeps are approximately equal for all curves, the charge/discharge behavior of these ACs in $NaNO_3$ should be highly reversible, which shows the promising potential in the application of EDLCs. On the other hand, the sequence of ACs with respect to decreasing the specific capacitance is: W-KOH-AC > P-KOH-AC > W-H_2O-AC > P-H_2O-AC. This result indicates that the charge storage within ACs is significantly affected by the density of oxygen functional groups formed on the ACs since the specific surface area of these four ACs is approximately the same (ca. 1050 m^2 g^{-1}) and the density of oxygen functional groups on the ACs is promoted by the KOH activation.

The dependence of voltammetric currents on the scan rate of CV was usually used to evaluate the reversibility and power property of electrode materials for the supercapacitor application [41–43]. Typical results for W-H_2O-AC and W-KOH-AC obtained at various potentials in 1 M $NaNO_3$ are shown in Fig. 5a and b, respectively. Note the linear dependence of the voltammetric currents on the scan rate of CV in both Fig. 5a and b. This phenomenon, in fact, is also found for P-H_2O-AC and P-KOH-AC in this electrolyte, indicating that the double-layer charge/discharge currents are typically capacitive-like. This result reveals a highly reversible charge/discharge response of the electric double layers, supporting the statement that the electrochemical reversibility of double-layer charge/discharge on these four AC-pasted electrodes in 1 M $NaNO_3$ is high. Accordingly, all AC-pasted electrodes in 1 M $NaNO_3$ are believed to exhibit high power characteristics, which meet one of the basic requirements for the electrode materials of supercapacitors.

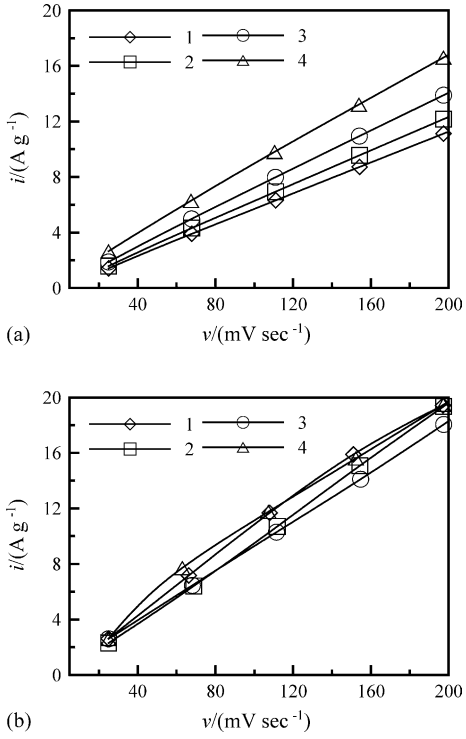

Fig. 5. Dependence of voltammetric currents for (a) W-H_2O-AC and (b) W-KOH-AC on the scan rate of CV, where currents were obtained at (1) 0.2, (2) 0.4, (3) 0.6, and (4) 0.8 V on the positive sweeps of CVs in 1 M $NaNO_3$.

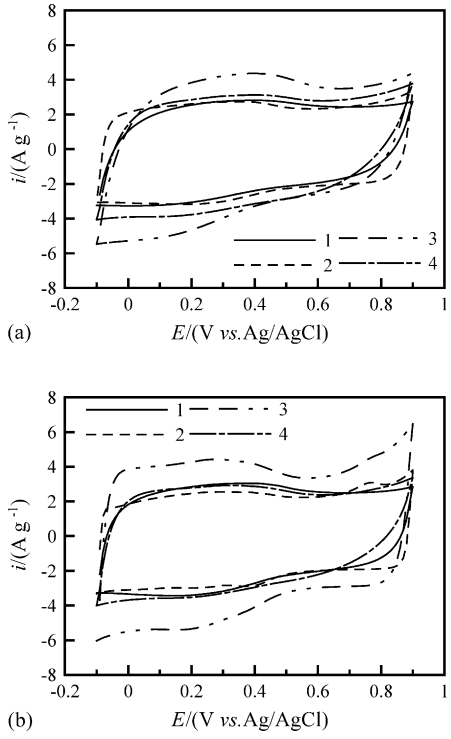

Fig. 6. Cyclic voltammograms of (1) W-H_2O-AC, (2) P-H_2O-AC, (3) W-KOH-AC, and (4) P-KOH-AC measured at 20 mV s^{-1} in (a) 1 M HNO_3 and (b) 0.5 M H_2SO_4.

In our previous work [44], steam-activated carbons were found to possess redox behavior in acidic electrolytes. This phenomenon is also examined in this work for the ACs prepared from fir wood or pistachio shells with the steam or KOH activation methods. Fig. 6a and b represents the typical cyclic voltammograms of W-H_2O-AC, P-H_2O-AC, W-KOH-AC, and P-KOH-AC measured at 20 mV s^{-1} in 1 M HNO_3 and 0.5 M H_2SO_4, respectively. From a comparison of Fig. 4 and Fig. 6a, three important features have to be mentioned. First, voltammetric currents measured in HNO_3 are higher than that measured in $NaNO_3$ for any specified AC. This result is attributable to two reasons: (i) the electrochemically accessible surface area of ACs is increased when an acidic electrolyte is employed and (ii) proton hopping in aqueous media [45] should favor the charge/discharge of electric double layers formed within the meso-/micropores of ACs. Second, distortion of CV curves from a rectangular shape is clearly found in Fig. 6a with the exception of curve 2 while all CVs curves in Fig. 4 are capacitive-like. This difference may be due to an increase in the (partially) accessible surface area for the formation of electric double layers in an acidic medium, delaying the movements of solvated ions within micropores under a medium scan rate of CV (e.g., 20 mV s^{-1}). Note that P-H_2O-AC exhibits capacitive *i–E* responses in both HNO_3 and $NaNO_3$, indicating that the capacitive characteristics of ACs should be significantly influenced by the raw material and the activation method. Third, there is a pair of wide but unclear peaks on all curves between −0.1 and 0.6 V, which were attributed to the presence of redox couples in this potential region [44]. This result suggests that certain functional groups formed on these ACs are electroactive in the acidic media, which become inactive in the neutral electrolyte (e.g., $NaNO_3$).

In Fig. 6b, the voltammetric behavior of W-H_2O-AC, P-H_2O-AC, and P-KOH-AC measured in 0.5 M H_2SO_4 is very similar to that obtained in the 1 M HNO_3 solution. However, the *i–E* responses of W-KOH-AC in the former solution are more suitable for the EDLC application because a more symmetric and rectangular-like CV curve as well as higher background currents are obtained. A higher capacitive current obtained in H_2SO_4 in comparison with that measured in HNO_3 may be is attributed to that the ion mobility of SO_4^{2-} is somewhat faster than that of NO_3^- [46]. However, this effect cannot explain the obvious difference in the *i–E* responses between W-KOH-AC and P-KOH-AC, implying that the double-layer capacitance of ACs is not only a function of the ion mobility but also influenced by the nature of ions. All the above results and discussion in this section demonstrate that the interactions at the electrolyte–AC interface should be very complicated, which are functions of pH of electrolytes, ion mobility, and functional groups formed on the surface of ACs. Based on the results and discussion for Fig. 6, W-KOH-AC in H_2SO_4 shows the best capacitive performance (i.e., highest specific capacitance and excellent reversibility) among all carbons prepared in this work.

The dependence of specific capacitance on the scan rate of CV for various ACs in 1 M $NaNO_3$, 1 M HNO_3, and 0.5 M H_2SO_4 are shown in Fig. 7a–c, respectively. Note that all

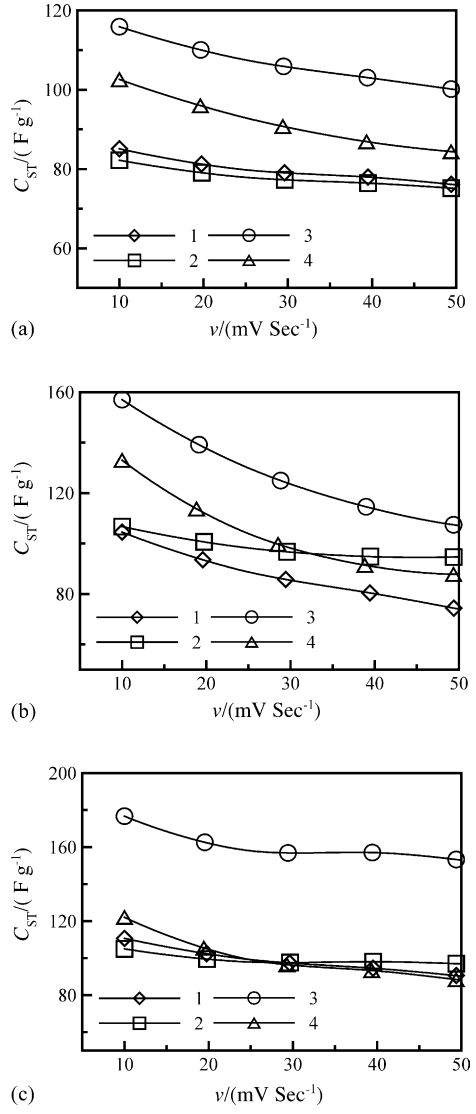

Fig. 7. Dependence of specific capacitance on the scan rate of CV in (a) 1 M $NaNO_3$, (b) 1 M HNO_3, and (c) 0.5 M H_2SO_4. All data were obtained from (1) W-H_2O-AC, (2) P-H_2O-AC, (3) W-KOH-AC, and (4) P-KOH-AC.

capacitance data shown in this work have been corrected with the capacitive contribution of graphite substrates although the capacitance of substrates is negligible. From these three figures, specific capacitance of ACs is monotonously decreased with increasing the scan rate of CV. This has been attributed to that the resistance of ion diffusion within certain micropores (especially the micropore surface partially accessible to electrolytes) becomes significant under a relatively high scan rate due to the differential depletion of the electrolyte concentration [9,13]. Accordingly, the electric double layers within these micropores are unable to be established completely under this relatively high charge/discharge rate. In addition, the proportion of these inaccessible micropores should be increased with increasing the scan rate of CV and a monotonous decrease in the specific capacitance of ACs is observed, accordingly.

From a comparison of curves 1–4 in Fig. 7a, an obvious decrease in the specific capacitance with increasing the scan rate of CV is clearly found for the KOH-activated carbons while this phenomenon is minor for the steam-activated carbons. These results are reasonably attributed to the larger mean pore size, the higher proportion of mesopores, and the ink-bottle type of pores within the steam-activated carbons. This statement is also supported by the results shown in Fig. 7b that the specific capacitance of P-H_2O-AC is almost independent on the scan rate of CV. This phenomenon is also visible in Fig. 7c although the dependence of specific capacitance on the scan rate of CV for all ACs is weaker in the H_2SO_4 solution in comparison with that measured in HNO_3. Therefore, from the excellent capacitive characteristics of P-H_2O-AC in both acidic and neutral media (see Figs. 4 and 6) and the very weak dependence of specific capacitance on the scan rate, P-H_2O-AC is believed to be the most suitable material for EDLCs in aqueous electrolytes. On the other hand, as discussed previously, W-KOH-AC shows the best capacitive performance in H_2SO_4 due to its highest specific capacitance and excellent reversibility.

From a comparison of Fig. 7b and c, a promotion in the specific capacitance is clearly found for the W-KOH-AC-pasted electrode when the supporting electrolyte is changed from HNO_3 to H_2SO_4. This phenomenon becomes more obvious as the scan rate of CV is increased. This result suggests the presence of a strong interaction between SO_4^{2-} and W-KOH-AC, which has also been proposed previously from the finding of obvious redox currents on curve 3 in Fig. 6b. In fact, the specific capacitance values of all activated carbons prepared in this work (from ca. 180 to 85 F g^{-1} for all ACs measured at 10 mV s^{-1} in various electrolytes) are larger than or comparable to that of some ACs studied previously, such as 80 F g^{-1} (specific surface area = 1200 m^2 g^{-1}) [47], 60–125 F g^{-1} (specific surface area from 1200 to 2315 m^2 g^{-1}) [15], 28–100 F g^{-1} (specific surface area from 1223 to 2571 m^2 g^{-1}) [11], and 90 F g^{-1} (specific surface area = 1500 m^2 g^{-1}) [48]. In addition, a certain AC with a high specific surface area (2371 m^2 g^{-1}) and a high pore volume (0.977 cm^3 g^{-1}) exhibited a specific capacitance of 27.9 F g^{-1} only [11]. The above comparison indicates the promising application potential of all ACs prepared in this work for EDLCs.

Based on all results and discussion in Fig. 7, the double-layer capacitance of steam-activated carbons is a weak function of the scan rate of CV in both neutral and acidic electrolytes, reasonably attributed to their intrinsic pore structure.

4. Conclusions

The specific capacitance of ACs was mainly determined by the electrochemically accessible surface area, due to the double-layer charge/discharge mechanism. The pore structure, surface functional groups, and raw materials of ACs, as well as pH and the supporting electrolyte were also found to

be the significant factors influencing the capacitive characteristics of ACs, especially obvious when the specific surface area of various ACs was kept approximately the same (ca. $1050\,m^2\,g^{-1}$) in this work. The double-layer capacitance of steam-activated carbons is a weak function of the scan rate of cyclic voltammetry in neutral and acidic electrolytes, due to their intrinsic pore structure (i.e., large mean pore size, relatively high mesoporous proportion and pores of the ink-bottle type). The development of pore structures is mainly determined by the activation methods, which were characterized by the t-plot method based on N_2 adsorption isotherms. The double-layer capacitance of ACs is not only a function of the ion mobility but also depends on the interactions between anions and ACs. Based on the excellent capacitive characteristics of P-H_2O-AC in both acidic and neutral media and the very weak dependence of specific capacitance on the scan rate of CV, P-H_2O-AC was demonstrated to be a very suitable electrode material for EDLCs in aqueous media. W-KOH-AC, however, was believed to be the best candidate for the electrode materials of EDLCs due to its excellent capacitive performance (i.e., highest specific capacitance (ca. $180\,F\,g^{-1}$ measured at $10\,mV\,s^{-1}$) and excellent reversibility) in H_2SO_4. This high specific capacitance is obviously larger than the typical value ($100\,F\,g^{-1}$) of activated carbons with specific surface areas equal to/above $1000\,m^2\,g^{-1}$.

Acknowledgment

The financial support of this work, provided by the National Science Council of the Republic of China, is gratefully acknowledged.

References

[1] D. Lozano-Castello, M.A. Lillo-Rodenas, D. Cazorla-Amoros, A. Linares-Solano, Carbon 39 (2001) 741.
[2] W.T. Tsai, C.Y. Chang, S.Y. Wang, C.F. Chang, S.F. Chien, H.F. Sun, Resour. Conservation Recycl. 32 (2001) 43.
[3] T. Kyotani, Carbon 38 (2000) 269.
[4] H. Shi, Electrochim. Acta 41 (1996) 1633.
[5] R.-L. Tseng, F.-C. Wu, R.-S. Juang, Carbon 41 (2003) 487.
[6] W.-T. Tsai, C.-Y. Chang, S.-L. Lee, Carbon 35 (1997) 1198.
[7] C.-T. Hsieh, H. Teng, Carbon 38 (2000) 863.
[8] H. Fujimoto, A. Mabuchi, K. Tokumitsu, T. Kasuh, Carbon 38 (2000) 871.
[9] B.E. Conway, Electrochemical Supercapacitors, Kluwer-Plenum Publishing Co., New York, 1999.
[10] L. Bonnefoi, P. Simon, J.F. Fauvarque, C. Sarrazin, J.F. Sarrau, A. Dugast, J. Power Sources 80 (1999) 149.
[11] D. Qu, H. Shi, J. Power Sources 74 (1998) 99.
[12] A. Burke, J. Power Sources 91 (2000) 37.
[13] K. Kinoshita, Carbon, in: Electrochemical and Physicochemical Properties, John-Wiley & Sons, New York, 1988.
[14] C. Niu, E.K. Sichel, R. Hoch, D. Moy, H. Tennent, Appl. Phys. Lett. 70 (1997) 1480.
[15] J. Gamby, P.L. Taberna, P. Simon, J.F. Fauvarque, M. Chesneau, J. Power Sources 101 (2001) 109.
[16] D. Qu, J. Power Sources 109 (2002) 403.
[17] R.L. McCreery, K.K. Cline, in: P.T. Kissinger, W.R. Heineman (Eds.), Laboratory Techniques in Electroanalytical Chemistry, Marcel Dekker, New York, 1996 (Chapter 10).
[18] F.-C. Wu, R.-L. Tseng, R.-S. Juang, J. Hazard. Mater. B69 (1999) 287.
[19] R.-S. Juang, F.-C. Wu, R.-L. Tseng, J. Colloid Interface Sci. 227 (2000) 437.
[20] Z. Hu, M.P. Srinivasan, Micropor. Mesopor. Mater. 27 (1999) 11.
[21] E.P. Barrett, L.G. Joyner, P.P. Halenda, J. Am. Chem. Soc. 73 (1951) 373.
[22] J.H. de Boer, B.C. Lippens, B.G. Linsen, J.C.P. Broekhoff, A. van den Heuvel, T.J. Osiga, J. Colloid Interface Sci. 21 (1966) 405.
[23] K.S.W. Sing, D.H. Everett, R.A.W. Haul, L. Moscou, R.A. Pierotti, J. Rouquerol, Pure Appl. Chem. 57 (1985) 603.
[24] K.S.W. Sing, Carbon 27 (1989) 5.
[25] E.F. Sousa-Aguilar, A. Liebsch, B.C. Chaves, A.F. Costa, Micropor. Mesopor. Mater. 25 (1998) 185.
[26] M.S. El-Geundi, Adsorpt. Sci. Technol. 15 (1997) 777.
[27] Y.C. Chiang, P.C. Chiang, E.E. Chang, J. Environ. Sci. Health A 33 (1998) 1437.
[28] D.M. Ruthven, Principles of Adsorption and Desorption Processes, Wiley, New York, 1984, pp. 55–58.
[29] K.S.W. Sing, D.H. Everett, R.A.W. Haul, L. Moscou, R.A. Pierotti, J. Rouquerol, T. Siemieniewska, Pure Appl. Chem. 57 (1985) 603.
[30] T.-C. Weng, H. Teng, J. Electrochem. Soc. 148 (2001) 368.
[31] H. Tamai, M. Kouzu, M. Morita, H. Yasuda, Electrochem. Solid State Lett. 6 (2003) 214.
[32] K. Gergova, N. Petrov, V. Minkova, J. Chem. Technol. Biotechnol. 56 (1993) 78.
[33] Z. Hu, M.P. Srinivasan, Micropor. Mesopor. Mater. 43 (2001) 267.
[34] F. Caturla, M. Molina-Sabio, F. Rodriguez-Reinose, Carbon 29 (1991) 999.
[35] A. Ahmadpour, D.D. Duong, Carbon 34 (1996) 471.
[36] R. Arriagada, R. Garcia, M. Molina-Sabio, F. Rodriguez-Reinoso, Micropor. Mater. 8 (1997) 123.
[37] V. Gome-Serrano, J. Pastor-Villegas, C.J. Duran-Valle, C. Valeneula-Calahorro, Carbon 34 (1996) 533.
[38] A.C. Lua, J. Guo, Colloids Surf., A 179 (2001) 151.
[39] P.-Z. Cheng, H. Teng, Carbon 41 (2003) 2057.
[40] Y. Otake, R.G. Jenkins, Carbon 31 (1993) 109.
[41] Y.-S. Chen, C.-C. Hu, Electrochem. Solid State Lett. 6 (2003) 210.
[42] K.-H. Chang, C.-C. Hu, J. Electrochem. Soc. 151 (2004) 958.
[43] C.-C. Hu, W.-C. Chen, Electrochim. Acta 49 (2004) 3469.
[44] F.-C. Wu, R.-L. Tseng, C.-C. Hu, C.-C. Wang, J. Power Sources 138 (2004) 351.
[45] A. Bard, L.R. Faulkner, Electrochemical Methods, Fundamentals and Applications, John-Wiley & Sons, New York, 1980.
[46] D.R. Crow, Principles and Applications of Electrochemistry, second ed., Chapman & Hall, London, 1974.
[47] L. Bonnefoi, P. Simon, J.F. Fauvarque, C. Sarrazin, A. Dugast, J. Power Sources 79 (1999) 37.
[48] A. Lewandowki, M. Zajder, E. Frackowiak, F. Beguin, Electrocheim. Acta 46 (2001) 2777.